Available online at www.sciencedirect.com
ScienceDirect
Journal of the European Ceramic Society 31 (2011) 2621–2627
www.elsevier.com/locate/jeurceramsoc

# Sintering behavior and mechanisms of NiO-doped 8 mol% yttria stabilized zirconia

X.C. Song [a], J. Lu [a], T.S. Zhang [b], J. Ma [a,*]

[a] School of Materials Science and Engineering, Nanyang Technological University, 50 Nanyang Avenue, Singapore 639798, Singapore
[b] School of Materials Science and Engineering, University of New South Wales, Sydney, NSW 2052, Australia

Received 30 August 2010; received in revised form 28 February 2011; accepted 16 March 2011
Available online 14 April 2011

**Abstract**

Sintering behavior and densification mechanisms of NiO-doped YSZ were investigated by using a dilatometer, combined with XRD, SEM and HRTEM characterization. The solubility of NiO in YSZ is found to be 0.5–1 mol% at 1500 °C by XRD, and TEM reveals that, beyond solubility limit, the undissolved NiO exists in the form of nano and/or micro-sized crystals depending on the doping amount. The sintering model was used to address the enhanced sintering of YSZ as a result of small additions of NiO. Lattice diffusion is examined to be the rate-determining mechanism for the intermediate-stage sintering of both undoped and NiO-doped YSZ. However, the apparent activation energy for densification of YSZ is reduced by ~70 kJ/mol upon NiO doping. It is concluded that the dissolved NiO contributes to the lowering of the activation energy and therefore the enhanced lattice diffusivity.


*Keywords:* NiO; Zirconia; Sintering kinetics; Apparent activation energy; Fuel cell

## 1. Introduction

Both YSZ and NiO are major constituents for fabricating solid oxide fuel cell (SOFC) systems. The former has been recognized to be the most promising electrolyte for commercial application, while YSZ–NiO composites are widely used as the starting materials for fuel cell anode. As a result, the interaction between YSZ and NiO has received considerable attention so far, especially the YSZ–NiO composites with high NiO contents (≥40 mol%).[1,2] With the preference to carry out co-sintering during the fabrication of SOFC stacks, the effect of small amounts of NiO (present as an impurity) on the performance of 8YSZ electrolytes has become increasingly important as the diffusion of $Ni^{2+}$ ions from the anode side towards the electrolyte is an unavoidable phenomenon.[3–5] Ni ions could diffuse tens of micrometers into the contacting YSZ layer when co-sintering is performed at 1550 °C for 6 h[3]; Joo et al.[4] have also reported that the Ni content in 10 mol% $Sc_2O_3$-stabilized zirconia (10SSZ) was found to be ~1.7 mol% after the co-sintering of a NiO layer/~10-μm thick 10SSZ film at 1600 °C for 3 h.

It is evident that the diffusion of small amount of NiO from the anode side will significantly affect not only the interface (anode/electrolyte) but also the entire electrolyte layer. Although a number of researchers have addressed the interaction of YSZ and small additions of NiO, most of the research work has focused on phase stabilization,[6] aging[7] and electrical properties.[6,8,9] It is well accepted that NiO doping helps in the stabilization of cubic phase and reduces the total conductivity. Recently, our work has also reported the effect of NiO on densification, grain growth and electrical properties (especially the grain-boundary conductivity) of YSZ in Si-free and Si contamination conditions.[10,11] Herle et al.[9] have also shown that small additions of NiO can significantly reduce the sintering temperature. However, thus far, no sintering mechanism study has been reported, which is essential for the understanding of the densification process to improve the final microstructure. In the present study, it is hence the aim to investigate the sintering behavior and mechanisms systematically, on 8YSZ with the NiO doping contents from 0 to 5 mol%. Moreover, several fundamental material properties, such as diffusion coefficient and activation energy, can also be obtained from the sintering study.

* Corresponding author.
*E-mail address:* asjma@ntu.edu.sg (J. Ma).

0955-2219/$ – see front matter © 2011 Elsevier Ltd. All rights reserved.
doi:10.1016/j.jeurceramsoc.2011.03.025

## 2. Experimental procedure

### 2.1. Sample preparation

High purity 8 mol% $Y_2O_3$–$ZrO_2$ (TZ-8Y, Tosoh Co., Tokyo, Japan) with a specific area of 16 $m^2/g$ was used as the starting materials. NiO dopant, ranging from 0.1 to 5 mol%, was loaded into 8YSZ powder via a wet chemical method using nickel nitrite as precursor. The 8YSZ powder and proper amount of nickel nitrite solution were thoroughly mixed to form slurry. The slurry was then dried and clacined at 600 °C for 1 h, followed by horizontal ball-milling for 12 h with Y-TZP balls in a polypropylene bottle. After drying, the obtained powders were firstly compacted in a stainless steel die to form cylindrical pellets (Φ 10 mm), which were subsequently subjected to cold isotropic pressing for 5 min under 200 MPa. The theoretical density ($\rho_T$) is estimated by the mixing law:

$$\rho_T = \frac{M_{YSZ} + xM_{NiO}}{M_{YSZ}/\rho_{YSZ} + xM_{NiO}/\rho_{NiO}} \quad (1)$$

where $x$ is molecular percentage of NiO, $M_{YSZ}$ and $M_{NiO}$ are molecular weight, and $\rho_{YSZ}$ (5.95 g/cm$^3$) and $\rho_{NiO}$ (6.27 g/cm$^3$) are theoretical density of 8YSZ and NiO, respectively. The resulted green densities were 49 ± 1% of the theoretical density.

### 2.2. Sintering and shrinkage

A horizontal push-rod dilatometer (DiL 402C, Netsch, Germany) is applied to monitor the dimension change of the samples during sintering. For each sample, five different heating rates between 2 and 15 °C/min were used. The temperature increased from room temperature (RT) to 1550 °C, and then decreased to RT with a rate of 20 °C/min. Prior to the sample measurement, baselines were created using sapphire as standard with the same heating profile so that instrument length variation could be calibrated. Thermal expansion was corrected with the thermal expansion coefficient which was determined from the cooling part of the shrinkage curve, and only corrected shrinkage was used in the following discussion. Nearly isotropic shrinkage was confirmed by evaluating change in both axial and radial dimension after dilatometric sintering. The instantaneous relative density ($\rho_i$) can be calculated from the following equation:

$$\rho_i = \left(\frac{1}{1 - \Delta L/L_0}\right)^3 \rho_g \quad (2)$$

where $\rho_g$ is the green relative density, and $\Delta L/L_0$ is the corrected shrinkage.

### 2.3. Phase and microstructural characterization

Phase identification was carried out on sintered samples using X-Ray diffractometer (SIEMENS D5005) with Cu Kα radiation (λ = 1.5418 Å) in the $20 \le 2\theta(^\circ) \le 85$ range. Rietveld analysis was applied to refine the structures, from which lattice parameters are calculated. Scanning electron microscope (SEM) is used to observe the microstructure. The samples were polished using a series of sand papers and diamond paste (0.3 μm) with polishing clothes, and then thermally etched to get the mirror-like surface. The etching temperature is 50 °C lower than its respective sintering temperature and the etching time is 30 min. Grain sizes are estimated by the linear intercept method over 200 grains. Actual grain size is determined by multiplying the apparent size by a factor of 1.56.[12] In addition, field emission transmission electron microscopy (FETEM, JEM-2100F) was used to observe the grain boundary structure. Specimens for TEM observation were prepared by mechanically grinding to a thickness of ~50 μm, followed by ion-milling for electron transparency. The local energy-dispersive spectroscopy (EDS) nano-analysis was performed to identify the elementary distribution.

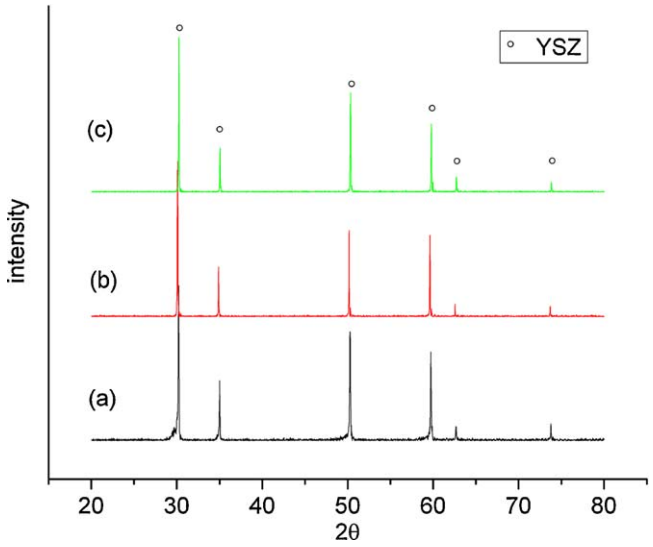


Fig. 1. XRD pattern of samples of (a) YSZ, (b) 0.5 mol% NiO-doped YSZ, (c) 5 mol% NiO-doped YSZ sintered at 1500 °C for 2 h.

### 2.4. Sintering model

The apparent activation energy ($Q$) can be determined from the following classic expression[13]:

$$\ln\left(TC\frac{d\rho}{dT}\right) = -\frac{Q}{RT} + \ln[f(\rho)] + \ln A - n \ln G \quad (3)$$

where $T$ is absolute temperature, $C$ is the heating rate, $R$ is gas constant, $f(\rho)$ is a function of density, $G$ is the grain size and $A$ is a material parameter that is insensitive to $G$, $\rho$, and $T$. The grain size power-law exponent, $n$, depends on whether sintering is controlled by lattice diffusion ($n = 3$) or by grain-boundary diffusion ($n = 4$). The Arrhenius plot of the left-hand side at a given density but different heating rates versus the reciprocal of $T$ gives the apparent activation energy.

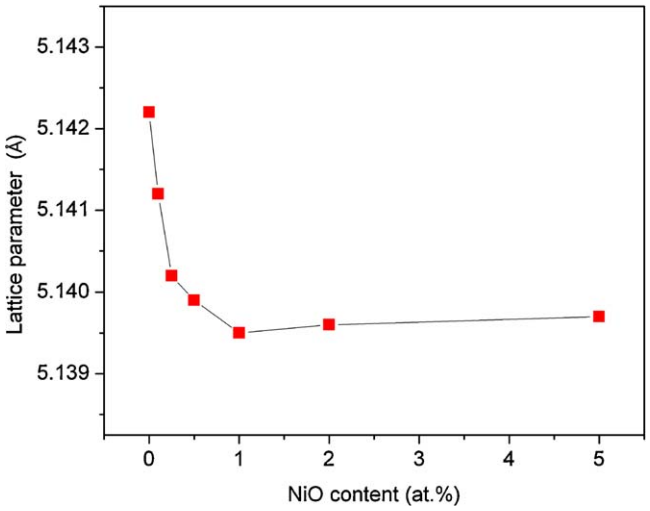


Fig. 2. lattice parameter varies with NiO content.

## 3. Results and discussion

### 3.1. Phase and microstructural analysis

Fig. 1 shows XRD patterns of undoped and NiO-doped samples. All the characteristic peaks belong to cubic phase of YSZ, except for the undoped YSZ, in which the peaks show some extent of broadening, probably due to the presence of small portion of tetragonal zirconia. The solubility of NiO in YSZ has been reported by a number of researchers,[3,5,17] but the literature data are quite scattered from less than 2 mol% to 10 mol%.[1,3] Therefore, the solubility of NiO in YSZ is re-evaluated by measuring the lattice parameter variation with NiO doping. From Fig. 2, the solubility limit is found to be 0.5–1 mol%. This value is smaller than that reported by Kuzjukevics[5] (1.5 mol%) at the same temperature. This should be ascribed to both the shorter sintering time and lower cooling rate used in the present case. On the other hand, it is interesting to mention that no NiO phase can be detected, even in the samples with 5 mol% NiO loading.

To detect the distribution of the undissolved NiO, the microstructure of 5 mol% NiO-doped sample was observed using FETEM, which was shown in Fig. 3(a). The microstructure reveals clearly the existence of secondary phases. Local EDS nano-analysis under scanning-transmission-electron-microscopy (STEM) mode was performed with a probe size of 1 nm, and the clustering of NiO micro-sized crystals (in the range of around 200 nm) can be easily identified from Fig. 3(b), which are mainly located near the grain boundaries. Fig. 3(c) shows the distribution of Zr element. There are several Zr-devoid areas confirmed, as indicated by the circles. Combining with the location of NiO crystals, the existence of residual pores could also be verified, which have been indicated by arrows in Fig. 3(a).

High resolution TEM micrographs for samples with different amount of NiO doping were examined. Fig. 4(a) shows the microstructure of 1.0 mol% NiO-doped sample sintered at 1300 °C for 2 h, and it was noted to have both very clean grain-interior and grain boundary. When the addition of NiO exceeds its solubility limit, the grain boundaries of YSZ becomes more disordered, which is considered to have been resulted from the enhanced segregation of NiO at the interface. Besides, the existence of nano-sized crystals of NiO was able to be detected; the typical existence is circled in Fig. 4(b). With the further addition of NiO, some of these nano-sized crystals cluster together and grow up. As a result, micro-sized crystals start to form, and that is the case found in the sample with 5 mol% NiO dopants (1500 °C-2 h), as shown in Fig. 3(b). All these findings manifest the fact that the undissolved NiO tends to exist in the form of nano and/or micro-sized crystals depending on the NiO doping amount.

### 3.2. Densification and grain growth

Fig. 5 shows the linear shrinkage as a function of temperature for the samples with different NiO contents. Upon NiO addition, the onset sintering temperature ($T_o$, where 0.5% shrinkage occurs) of YSZ shifts to a lower temperature. For example, $T_o$ is 1095 °C for undoped 8YSZ, while it decreases to 1036 °C for 0.5 mol% NiO-doped sample. The shrinkage of 8YSZ becomes more enhanced as the amount of doped NiO was increased to 0.5 mol%. However, further addition of NiO results in little influence on the densification behavior of YSZ; the shrinkage curve exhibits almost the identical track with that of 0.5 mol% NiO-doped sample. For clarity, the linear shrinkage curves of YSZ with 1 mol% and 5 mol% NiO doping are not shown here. Considering the coincidence of this amount with the solubility limit (0.5–1 mol%), we infer that the enhanced sintering should somewhat be related to the dissolution of NiO into YSZ lattice. Fig. 6 shows the densification rate with temperature. The temperature, at which maximum shrinkage rate occurs ($T_{max}$), decreases

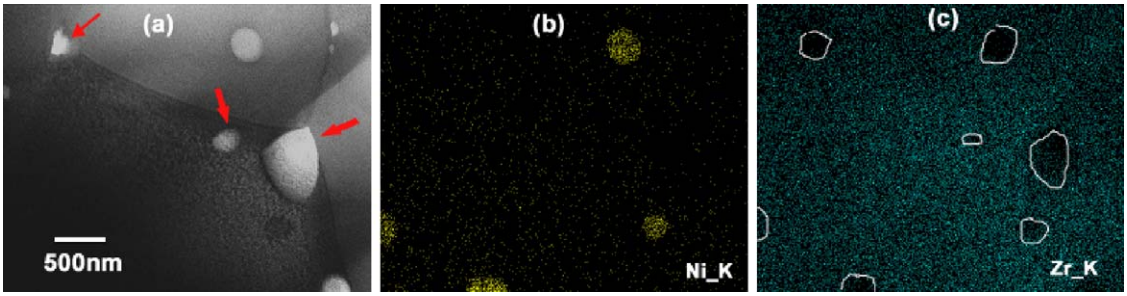


Fig. 3. (a) Microstructure of 5.0 mol% NiO-doped YSZ sintering at 1500 °C for 2 h; arrows indicate the location of pores, (b) local EDS mapping of Ni using Ni_K peaks, and (c) local EDS mapping of Zr; circled areas represent Zr-devoid regions.

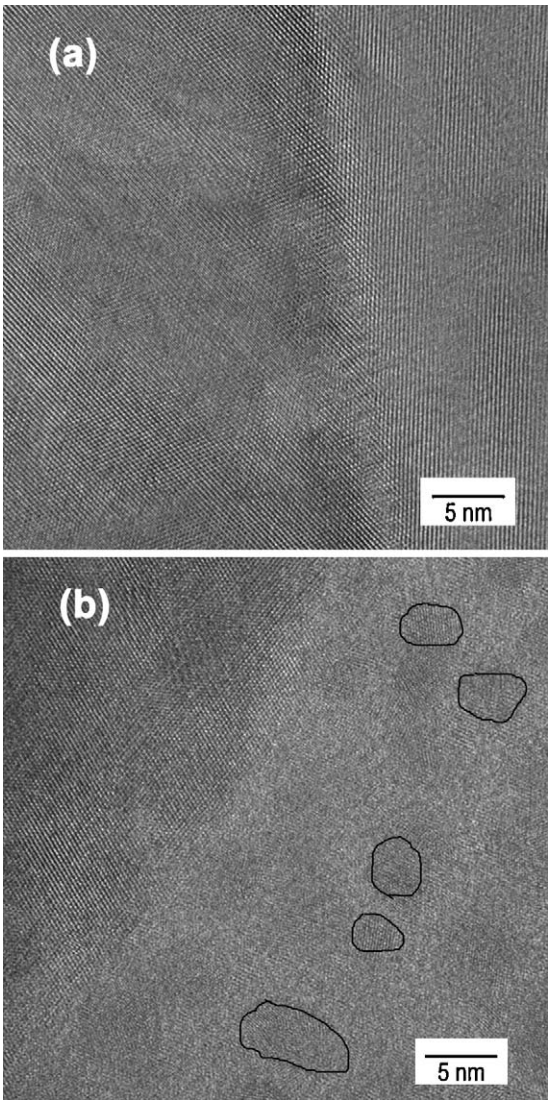


Fig. 4. High-resolution transmission electron microscopy image of (a) 1.0 mol% NiO-doped YSZ (1300 °C 2 h) and (b) 5.0 mol% NiO-doped YSZ (1500 °C 2 h); the circled area indicates nano-sized crystals of secondary.

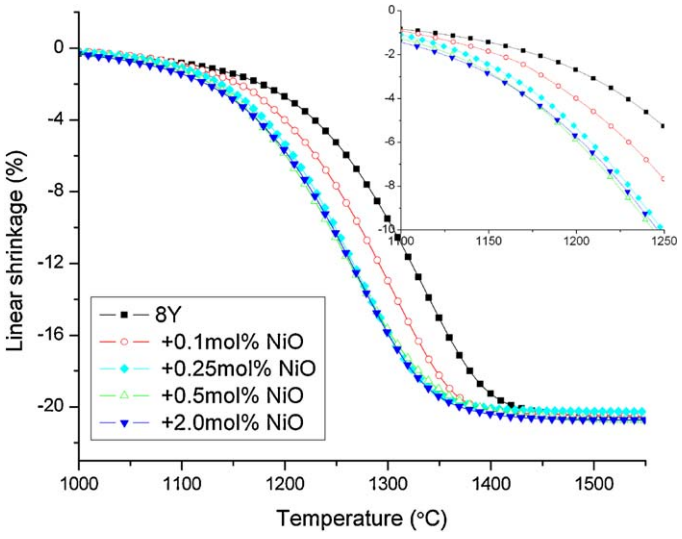


Fig. 5. Linear shrinkage versus temperature for (■) YSZ; (◯) 0.1 mol%, (♦) 0.25 mol%, (△) 0.5 mol%, (▼) 2 mol% NiO-doped YSZ, under the heating rate of 5 °C/min; the inset figure shows the enlarged part of the initial stage of sintering.

from 1346 °C to 1267 °C for the 0.5-mol% doped samples. This reduction of sintering temperature by 79 °C reflects clearly the sintering-promoting role of NiO for YSZ. Similar observation was also reported elsewhere.[10,17]

On the other hand, the grain growth of YSZ is initially promoted with the addition of NiO up to ~1 mol%, and then inhibited with further addition of NiO (Figs. 7 and 8). The enhanced grain growth is also reckoned to be closely related to the solubility of NiO in the zirconia lattice, which will be discussed later. For high Ni content doping of 1–5 mol%, both pores and NiO second phase in the microstructure contribute to the "solute dragging effect". As a result, migration of grain boundaries are restricted.[18]

SEM observation suggests lots of pores exist both within the grain interior and at the grain boundaries in the highly doped YSZ (Fig. 5(d)). Preliminary results have revealed that only ~0.5–1 mol% NiO can dissolve in the lattice of zirconia, and the undissolved NiO is found to exist in both nano and micro-sized crystals in the sample with 5 mol% NiO. The clustering of NiO was expected to initiate at the interface, but during the final-stage of sintering, the formed clusters were involved into the migration of grain boundaries, and are thus left behind within the bulk of grains; meanwhile, the clusters continue to grow up (Fig. 3(b)). This could partly explain the porous structure in the 5-mol% doped YSZ, because the localized sintering of NiO will induce stress to its surroundings, leaving residual pores at both interface and grain interior. However, there are also many other factors responsible for the residual pores. One possibility, for instance, is that the grain boundary characteristic has been changed by NiO segregation (Fig. 4), and consequently is the change of interface energy, which has significant influence on the mobility of boundary/pores.

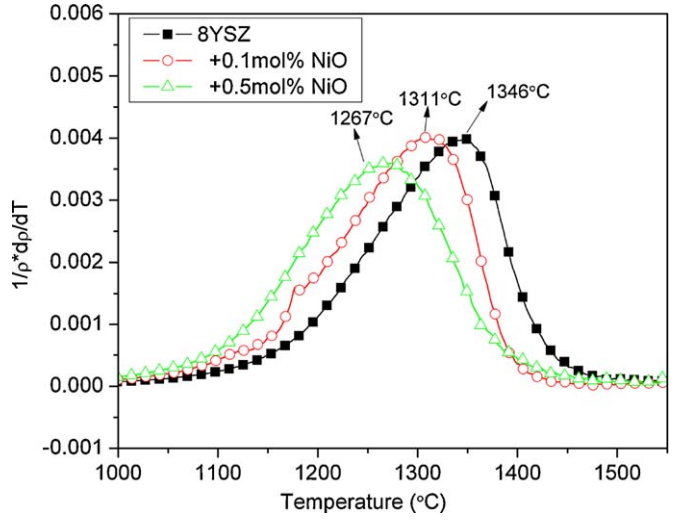


Fig. 6. Densification rate versus temperature for (■) 8YSZ; (◯) 0.1 mol% NiO-doped YSZ, (△) 0.5 mol% NiO-doped YSZ; the heating rated is 5 °C/min.

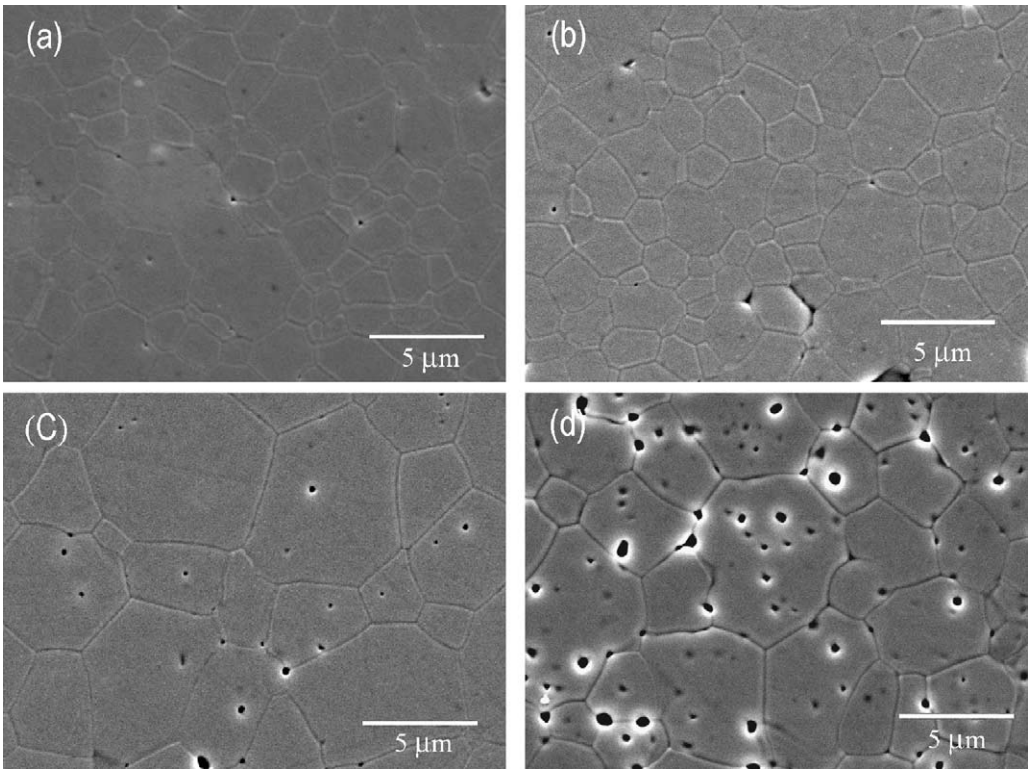


Fig. 7. SEM micrographs of samples sintered at 1400 °C for 2 h: (a) YSZ; (b) 0.25 mol% NiO-doped YSZ, (c). 1 mol% NiO-doped YSZ, (d) 5 mol% NiO-doped YSZ.

### 3.3. Densification kinetics

Fig. 9 represents the Arrhenius type dependence of densification rate on reciprocal of temperature at constant densities for undoped and 0.5 mol% NiO-doped YSZ. The very good linear fit to both data implies that the model can be used with confidence. The variation of apparent activation energy, $Q$, verses relative density has been shown in detail in Fig. 10. It is found that $Q$ decreases abruptly from early-stage (<56% relative density) to the intermediate-stage of sintering (≥56% relative density). Hence, the apparent activation energies are averaged over individual densification stage. During the early stage of sintering, the activation energy is determined to be $691 \pm 60$ kJ/mol and $660 \pm 93$ kJ/mol, while it is $572 \pm 15$ kJ/mol and $501 \pm 5$ kJ/mol in the intermediate stage for undoped and 0.5 mol% NiO-doped YSZ, respectively. The activation energy is reduced by about 70 kJ/mol with the addition of 0.5 mol% NiO. The obtained activation energy for undoped YSZ is in good agreement with those reported in literature.[19–21] However, this is the first time, to our best knowledge, that the densification activation energy of NiO-doped YSZ is reported.

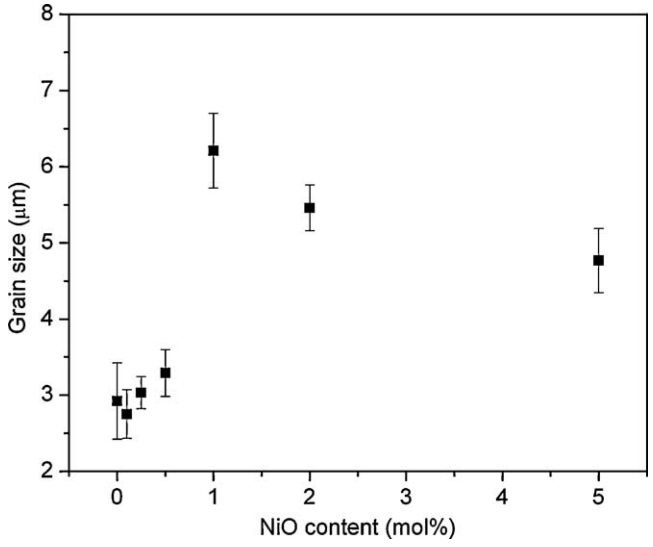


Fig. 8. Grain size of 8YSZ as a function of NiO doping content, sintered at 1400 °C for 2 h.

From the literature, most of the reported activation energy for lattice diffusion (LD) during the sintering of $Y_2O_3$–$ZrO_2$ is in the range of 460–616 kJ/mol,[22–26] while the activation energy for grain boundary diffusion (GBD) is most likely between 309 and 373 kJ/mol.[25,26] In this study, during the intermediate-stage of sintering, the activation energies for both undoped YSZ and 0.5 mol% NiO-doped YSZ are comparable to those values reported as lattice diffusion.[22–26] Therefore, the dominant sintering mechanism is most appropriately assigned to lattice diffusion. On the other hand, the activation energy for the early-stage of sintering is higher than both LD and GBD. It should be noted that surface diffusion has been neglected in the model. As pointed out, surface diffusion usually increases the apparent activation energy, yet does not give densification.[27] Hence, the anomalously high activation energy in the early stage was probably originated from the effect of surface diffusion.

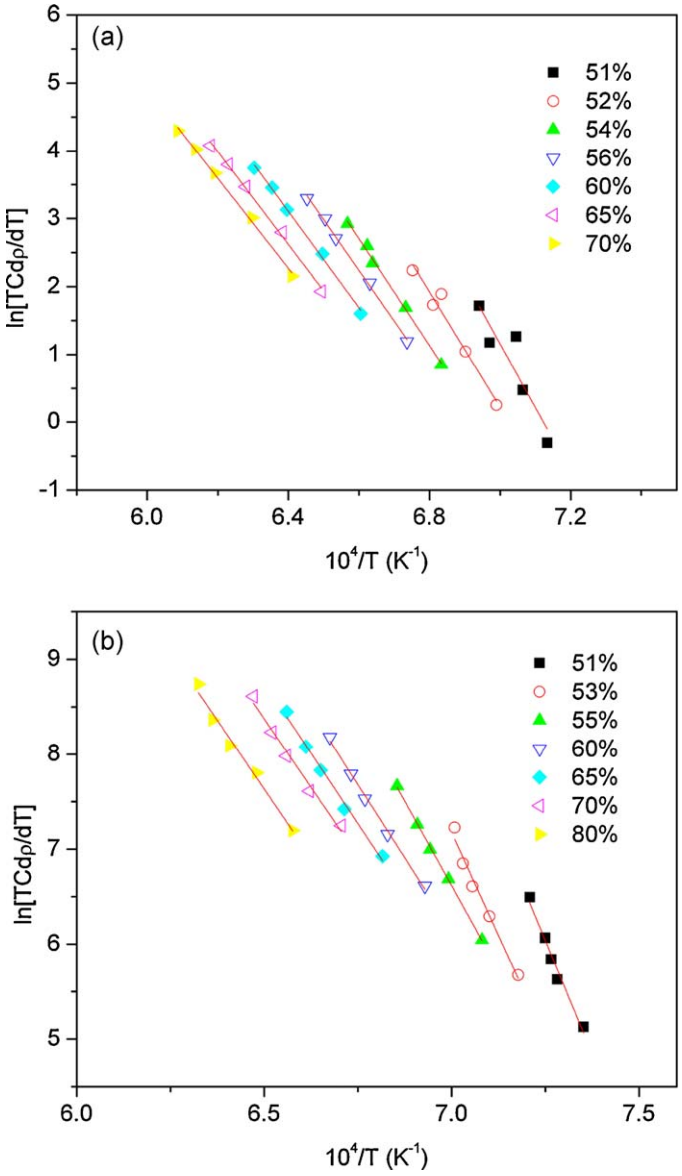


Fig. 9. Arrhenius plots of densification data for estimation of apparent activation energy: (a) 8YSZ; (b) 0.5 mol% NiO-doped YSZ. The numbers represent the constant relative density.

The doping of NiO into YSZ does not change the densification mechanism, i.e. lattice diffusion; however, the activation energy is reduced. The interconnection between enhanced sintering and dissolution of NiO has been discussed in Section 3.2. Concerning the influence of dopants on the lattice diffusivity, the possible factors are as follows: (1) the smaller ionic size of dopants cations relieves the elastic stress and "facilitates" fast diffusive paths; (2) compensating point defects are generated by cations of different valence; (3) chemical bonding strength between Zr–O is weakened through the interaction of outer shells' electrons.[28] For the case of YSZ, the first factor can be steadily established, since the ionic size of $Ni^{2+}$ (0.69 Å) is smaller than both $Zr^{4+}$ (0.84 Å) and $Y^{3+}$ (1.019 Å). It has been reported that $Zr^{4+}$ diffusion via cation vacancies, i.e. $V''''_{Zr}$, is the rate-limiting step,[26] however, the creation of $V''''_{Zr}$ is not possible by lower valence cation doping. The change of chemical bonding state is difficult to obtain experimentally, but it is probably one of the reasons for enhanced grain boundary diffusion. Further investigation by first-principle molecular orbital calculation will be required to confirm this effect.

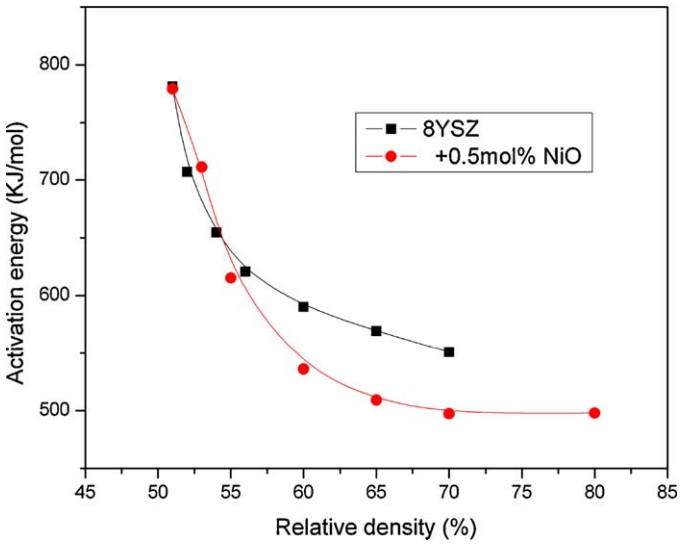


Fig. 10. Activation energy as a function of relative density (■) YSZ; (●) 0.5 mol% NiO-doped YSZ.

## 4. Conclusions

(1) The addition of a small amount of NiO was found to lower the onset sintering temperature of YSZ, and both early and intermediate-stage densification of YSZ is enhanced. NiO doping also promotes grain growth of YSZ and 1 mol% NiO doping is found to be most effective; however, grain growth of YSZ was observed to have slown down when doped with higher amount of NiO (>1 mol%).

(2) Intermediate-stage sintering of both undoped and NiO-doped YSZ was examined to be dominated by lattice diffusion. The apparent activation energy for the densification of YSZ is reduced by ~70 kJ/mol when 0.5 mol% NiO is added.

(3) XRD analysis has shown that ~0.5–1 mol% NiO can dissolve into YSZ lattice at 1500 °C. Beyond solubility limit, the undissolved NiO was found to exist in the form of nano and/or micro-sized crystals depending on the doping amount. The solubility of NiO is closely associated with the enhancement of sintering, grain growth, and the lowering of sintering activation energy. The enhanced lattice diffusivity is found to be caused by the dissolution of NiO into YSZ lattice.

## References

1. Park YM, Choi GM. Mixed ionic and electronic conduction in YSZ–NiO composite. *J Electrochem Soc* 1999;**146**(3):883–9.
2. Fonseca FC, de Florio DZ, Esposito V, Traversa E, Muccillo ENS, Muccillo R. Mixed ionic–electronic YSZ/Ni composite for SOFC anodes with high electrical conductivity. *J Electrochem Soc* 2006;**153**(2):A354–60.

3. Delaforce PM, Yeomans JA, Filkin NC, Wright GJ, Thomson RC. Effect of NiO on the phase stability and microstructure of yttria-stabilized zirconia. *J Am Ceram Soc* 2007;**90**(3):918–24.
4. Joo JH, Choi GM. Effect of Ni doping on the phase stability and conductivity of scandia-stabilized zirconia. *Solid State Ionics* 2009;**180**(2–3): 252–6.
5. Kuzjukevics A, Linderoth S. Interaction of NiO with yttria-stabilized zirconia. *Solid State Ionics* 1997;**93**(3–4):255–61.
6. Kondo H, Sekino T, Kusunose T, Nakayama T, Yamamoto Y, Niihara K. Phase stability and electrical property of NiO-doped yttria-stabilized zirconia. *Mater Lett* 2003;**57**(9–10):1624–8.
7. Mori H, Wen C-j, Otomo J, Eguchi K, Takahashi H. Investigation of the interaction between NiO and yttria-stabilized zirconia (YSZ) in the NiO/YSZ composite by temperature-programmed reduction technique. *Appl Catal A: Gen* 2003;**245**(1):79–85.
8. Linderoth S, Bonanos N, Jensen KV, Bilde-Sørensen JB. Effect of NiO-to-Ni transformation on conductivity and structure of yttria-stabilized $ZrO_2$. *J Am Ceram Soc* 2001;**84**(11):2652–6.
9. Van Herle J, Vasquez R. Conductivity of Mn and Ni-doped stabilized zirconia electrolyte. *J Eur Ceram Soc* 2004;**24**(6):1177–80.
10. Zhang TS, Chan SH, Kong LB, Sheng PT, Ma J. Synergetic effect of NiO and $SiO_2$ on the sintering and properties of 8 mol% yttria-stabilized zirconia electrolytes. *Electrochim Acta* 2009;**54**(3):927–34.
11. Zhang TS, Du ZH, Li S, Kong LB, Song XC, Lu J, et al. Transitional metal-doped 8 mol% yttria-stabilized zirconia electrolytes. *Solid State Ionics* 2009;**180**(23–25):1311–7.
12. Mendelson M. Average grain size in polycrystalline ceramics. *J Am Ceram Soc* 1969;**52**(8):443–6.
13. Wang JD, Raj R. Estimate of the activation-energies for boundary diffusion from rate-controlled sintering of pure alumina, and alumina doped with zirconia or titania. *J Am Ceram Soc* 1990;**73**(5):1172–5.
17. Shueiyuan C, Pouyan S, Dershin G. Growth kinetics of sintered NiO/$ZrO_2$ (5 mol.% $Y_2O_3$) composites. *Mater Sci Eng A* 1992;**158**(2):251–8.
18. Santos AP, Domingues RZ, Kleitz M. Grain boundary blocking effect in tetragonal yttria stabilized zirconia. *J Eur Ceram Soc* 1998;**18**(11):1571–8.
19. Zhang TS, Chan SH, Wang W, Hbaieb K, Kong LB, Ma J. Effect of Mn addition on the densification, grain growth and ionic conductivity of pure and $SiO_2$-containing 8YSZ electrolytes. *Solid State Ionics* 2009;**180**(1):82–9.
20. Wang JD, Raj R. Activation-energy for the sintering of 2-phase alumina zirconia ceramics. *J Am Ceram Soc* 1991;**74**(8):1959–63.
21. Matsui K, Ohmichi N, Ohgai M, Enomoto N, Hojo J. Sintering kinetics at constant rates of heating: effect of $Al_2O_3$ on the initial sintering stage of fine zirconia powder. *J Am Ceram Soc* 2005;**88**(12):3346–52.
22. Matsui K, Ohmichi N, Ohgai M, Enomoto N, Hojo J, Sintering. Kinetics at constant rates of heating: effect of alumina on the initial sintering stage of yttria-stabilized cubic zirconia powder. *J Ceram Soc Jpn* 2006;**114**(9):763–8.
23. Chien FR, Heuer AH. Lattice diffusion kinetics in $Y_2O_3$-stabilized cubic $ZrO_2$ single crystals: a dislocation loop annealing study. *Philos Mag A* 1996;**73**(3):681–97.
24. Martinez-Fernandez J, Jimenez-Melendo M, Dominguez-Rodriguez A, Heuer AH. High-temperature creep of yttria-stabilized zirconia single crystals. *J Am Ceram Soc* 1990;**73**(8):2452–6.
25. Taylor MA, Kilo M, Borchardt G, Weber S, Scherrer H. $^{96}Zr$ diffusion in polycrystalline scandia stabilized zirconia. *J Eur Ceram Soc* 2005;**25**(9):1591–5.
26. Kilo M, Borchardt G, Lesage B, Kaïtasov O, Weber S, Scherrer S. Cation transport in yttria stabilized cubic zirconia: $^{96}Zr$ tracer diffusion in $(Zr_xY_{1-x})O_{2-x/2}$ single crystals with $0.15 \leq x \leq 0.48$. *J Eur Ceram Soc* 2000;**20**(12):2069–77.
27. Sethi G, Park SJ, Johnson JL, German RM. Linking homogenization and densification in W–Ni–Cu alloys through master sintering curve (MSC) concepts. *Int J Refract Met Hard Mater* 2009;**27**(4):688–95.
28. Boniecki M, Natanzon Y, Lodziana Z. Effect of cation doping on lattice and grain boundary diffusion in superplastic yttria-stabilized tetragonal zirconia. *J Eur Ceram Soc* 2010;**30**(3):657–68.